Polymer 51 (2010) 4368–4374

Contents lists available at ScienceDirect

Polymer

journal homepage: www.elsevier.com/locate/polymer

Formation and characterization of core-sheath nanofibers through electrospinning and surface-initiated polymerization

Liwen Ji, Zhan Lin, Ying Li, Shuli Li, Yinzheng Liang, Ozan Toprakci, Quan Shi, Xiangwu Zhang*

Fiber and Polymer Science Program, Department of Textile Engineering, Chemistry and Science, North Carolina State University, Raleigh, NC 27695-8301, USA

ARTICLE INFO

Article history:
Received 3 June 2010
Received in revised form
20 July 2010
Accepted 24 July 2010
Available online 1 August 2010

Keywords:
Polyacrylonitrile
Polypyrrole
Electrospinning

ABSTRACT

Novel core-sheath nanofibers, composed of polyacrylonitrile (PAN) core and polypyrrole (PPy) sheath with clear boundary between them, were fabricated by electrospinning PAN/$FeCl_3 \cdot 6H_2O$ bicomponent nanofibers and the subsequent surface-initiated polymerization in a pyrrole-containing solution. By adjusting the concentration of $FeCl_3 \cdot 6H_2O$, the surface morphology of PPy sheath changed from isolated agglomerates or clusters to relatively uniform thin-film structure. Thermal properties of PAN-PPy core-sheath nanofibers were also characterized. Results indicated that the PPy sheath played a role of inhibitor and retarded the complex chemical reactions of PAN during the carbonization process.

1. Introduction

In the last decade, electrospinning has revived as a fascinating choice to assemble polymer nanofibers with various morphologies and functionalities due to its simplicity and cost effectiveness, along with environmental benignity [1–5]. The unique structural features, such as high surface-area-to-volume ratio, extremely long length, and complex porous structure, etc., of electrospun nanofibers make them suitable for various applications, including but not limited to tissue engineering scaffolds [6], drug delivery systems [7], sensors [8], environmental protection [9,10], nanoscale electronic and optoelectronic devices [11], catalysts [12,13], and electrode materials for energy storage and conversion systems [14,15]. Nanofibers made from simple electrospinning usually exhibit a solid interior and smooth surface. However, electrospun nanofibers with unique secondary structures can also be prepared in order to obtain exceptional functionalities [3,16]. Especially, electrospun core-sheath nanofibers have gained extraordinary attention due to the combination of the characteristics of two different components into one integrity in the axial or radial direction [16,17]. For example, Wei et al. observed the formation of core-sheath polyaniline (PANI)-polycarbonate (PC) nanofibers, derived from the micro-phase separation after the electrospinning of PANI/PC blend solutions [16,17]. Core-sheath nanofibers can also be fabricated by other methods, such as co-electrospinning two different polymer solutions via a spinneret comprising two coaxial capillaries [18,19], template-directed growth [20], surface-initiated atom transfer radical polymerization (ATRP) [21], and the so-called 'emulsion electrospinning' [22].

Electrospun core-sheath nanofibers containing conductive polymers, such as PPy, are fundamentally important and have wide applications because of their high electrical conductivity and good stability under ambient conditions [23–28]. Most conductive polymers are expensive and hard to be electrospun because of their poor solubility in most solvents. The preparation of core-sheath nanofibers through indirect methods combined with electrospinning technique is a feasible approach to obtain conductive polymer nanofiber materials, which may have wide technological applications in electrical, optical, thermal, and magnetic materials and devices. In this paper, we report the generation of PAN-PPy core-sheath nanofibers through electrospinning of PAN and the subsequent surface-initiated polymerization of pyrrole. The surface morphologies and the thermal properties of these fibers are also characterized.

2. Experimental

2.1. Materials

PAN was purchased from Fisher Scientific. $FeCl_3 \cdot 6H_2O$, pyrrole, N, N-dimethylformamide (DMF) and tetrahydrofuran (THF) were purchased from Sigma–Aldrich. All these chemicals were used without further purification. DMF solutions of PAN (8 wt %) containing different amount of $FeCl_3 \cdot 6H_2O$ (0, 1, 2, 5, and 10 wt %) were prepared at 60 °C with mechanical stirring for at least 48 h.

* Corresponding author. Tel.: +1 919 515 6547.
E-mail address: xiangwu_zhang@ncsu.edu (X. Zhang).

0032-3861/$ – see front matter © 2010 Elsevier Ltd. All rights reserved.
doi:10.1016/j.polymer.2010.07.042

2.2. Electrospinning of PAN/$FeCl_3 \cdot 6H_2O$ nanofibers

A variable high voltage power supply (Gamma ES40P-20 W) was used to provide a high voltage (around 10 kV) for electrospinning with 0.5 ml h^{-1} flow rate and 15 cm needle-to-collector distance. The electrospun PAN/$FeCl_3 \cdot 6H_2O$ nanofibers were accumulated on an aluminum foil surface and collected as a fibrous mat.

2.3. Fabrication of PAN-PPy core-sheath nanofibers

PPy was obtained on electrospun PAN nanofibers by surface-initiated polymerization of pyrrole monomers using Fe^{3+} as an oxidant. PAN nanofibers (about 2 g) were immersed in 20 ml THF solution of pyrrole (5 ml), followed by adding about 20 ml HCl (0.1 M) aqueous solution. The mixture was shaken vigorously for 0.5 h. The polymerization of pyrrole was initiated by the Fe^{3+} in electrospun PAN nanofibers at room temperature. During the polymerization, PAN nanofibers changed appearance from white to dark as the result of the formation of black PPy on the surfaces. Nanofibers with PPy sheath were then washed with THF and acetone for several times to remove the non-reacted pyrrole monomers.

2.4. Carbonization of PAN-PPy core-sheath nanofibers

PAN-PPy core-sheath bicomponent nanofibers were first stabilized in air environment at 280 °C for 6 h (heating rate was 5 °C min^{-1}) and then carbonized at 600 °C for 8 h in argon atmosphere (heating rate was 2 °C min^{-1}).

2.5. Morphologies of nanofibers

The morphology of electrospun pure PAN, PAN/$FeCl_3 \cdot 6H_2O$, PAN-PPy core-sheath nanofibers, and the corresponding carbonized nanofibers were evaluated using scanning electron microscopy (JEOL 6400F Field Emission SEM at 5 kV). PAN-PPy core-sheath nanofibers were also characterized using transmission electron microscopy (TEM) (FEI Tecnai G2 Twin) with an accelerating voltage of 120 kV.

2.6. ATR-FTIR spectroscopy

Pure PAN, PAN/10 wt% $FeCl_3 \cdot 6H_2O$ and the corresponding PAN-PPy core-sheath nanofibers were evaluated using attenuated total reflection fourier transform infrared spectroscopy (ATR-FTIR). The spectra were collected from an FTIR spectrometer (Nicolet 560) in the wavenumber range of 3700–700 cm^{-1} at room temperature. Sixty-four scans were conducted to achieve an adequate signal-to-noise ratio.

2.7. Thermal analysis

Thermal properties of pure PAN, PAN/10 wt% $FeCl_3 \cdot 6H_2O$ and the corresponding PAN-PPy core-sheath nanofibers were evaluated using differential scanning calorimetery (DSC) from 25 to 400 °C at a heating rate of 10 °C min^{-1} in a nitrogen atmosphere (Thermal InstrumentsDSC-Q2000). Thermo-gravimetric analysis (TGA) was also used to determine the weight loss of these nanofibers at 10 °C min^{-1} from 25 to 800 °C in air environment (Thermal Instruments TGA-Q500).

3. Results and discussion

3.1. Surface morphologies of the prepared nanofibers

Fig. 1 presents the SEM images of electrospun PAN/$FeCl_3 \cdot 6H_2O$ composite nanofibers with different $FeCl_3 \cdot 6H_2O$ contents. All

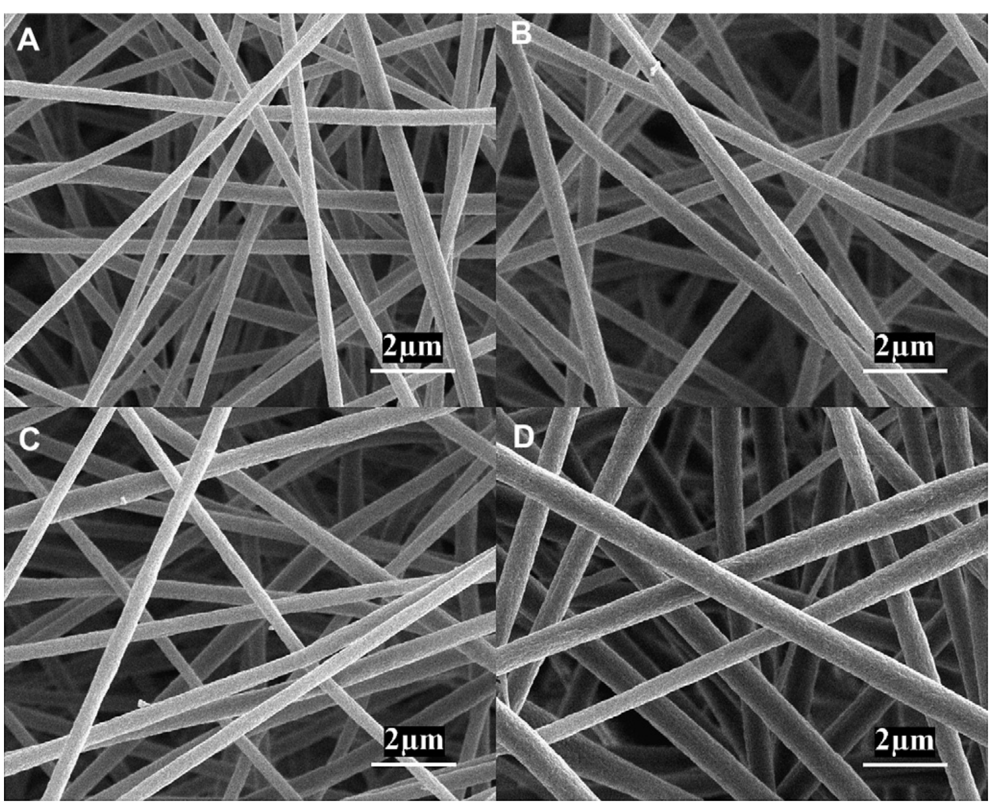

Fig. 1. SEM images of PAN/$FeCl_3 \cdot 6H_2O$ nanofibers with different $FeCl_3 \cdot 6H_2O$ contents: (A) 1, (B) 2, (C) 5 and (D) 10 wt%.

nanofibers present relatively uniform morphology and randomly oriented structure. With the increase of $FeCl_3 \cdot 6H_2O$ content, the fiber diameter increases, which may be the result of the changes in solution viscosity, surface tension, and conductivity caused by the addition of ions [3,10,29,30]. The uniform fiber morphology is totally changed after the surface-initiated polymerization of pyrrole (Fig. 2). From Fig. 2, it is seen that after the polymerization, PAN/1 wt% $FeCl_3 \cdot 6H_2O$ nanofibers show some non-uniformities and irregularities. When the $FeCl_3 \cdot 6H_2O$ content increases to 2 wt%, distinct PPy clusters or agglomerates appear on fiber

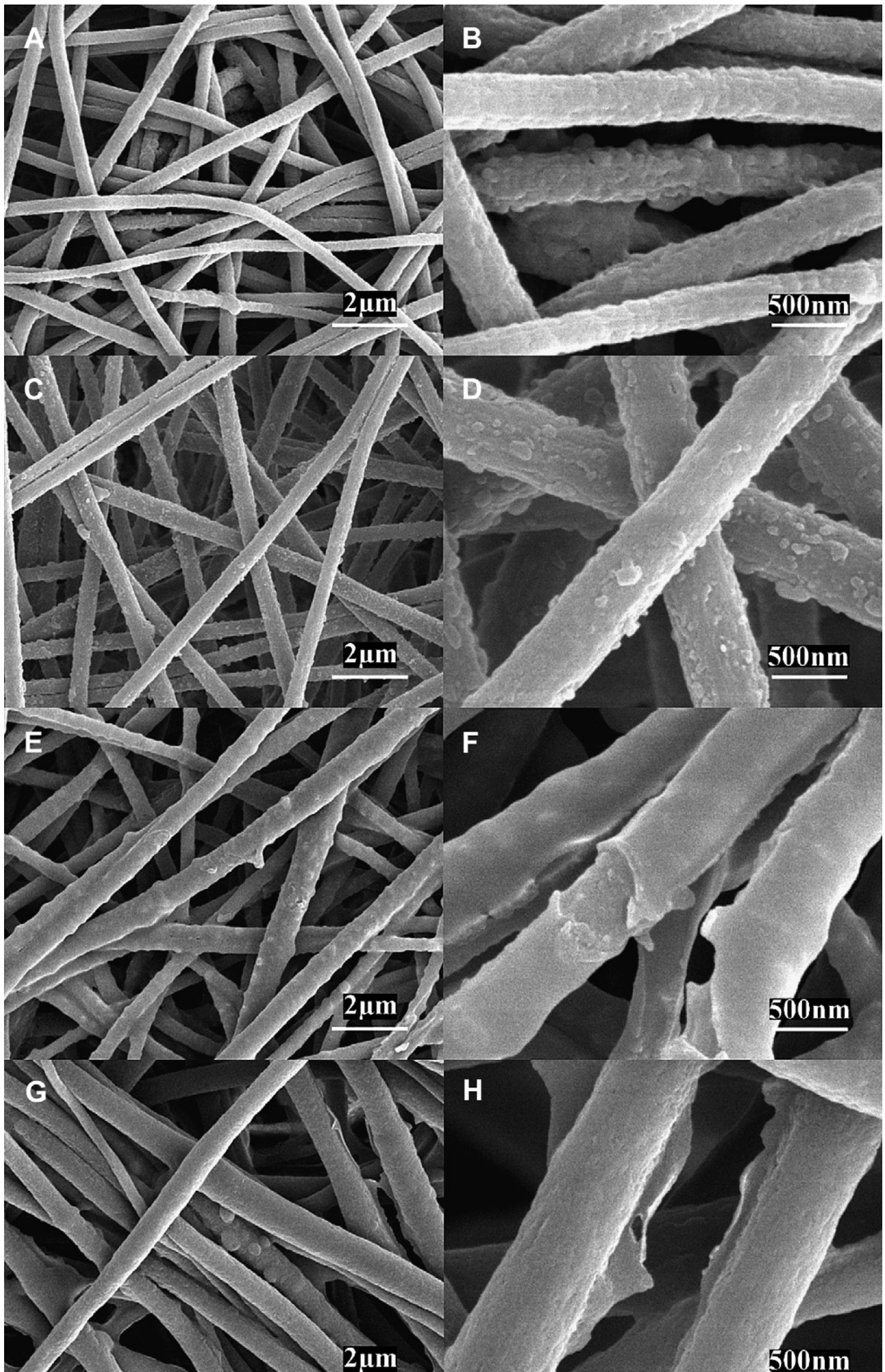

Fig. 2. SEM images of PAN-PPy core-sheath nanofibers made from electrospun PAN/$FeCl_3 \cdot 6H_2O$ with different $FeCl_3 \cdot 6H_2O$ contents: (A, B) 1, (C, D) 2, (E, F) 5 and (G, H) 10 wt%.

surface. At 5 wt % $FeCl_3 \cdot 6H_2O$ content, the PPy phase turns to a continuous and elongated fibrillar sheath structure wrapping the electrospun PAN/$FeCl_3 \cdot 6H_2O$ nanofiber surface. The PPy sheath can also been seen from the PAN/10 wt % $FeCl_3 \cdot 6H_2O$ nanofibers after the polymerization. The formation of core-shell nanofiber structure is further confirmed by Fig. 3, which shows the TEM images of PAN/$FeCl_3 \cdot 6H_2O$ nanofibers (5 and 10 wt % $FeCl_3 \cdot 6H_2O$) after the polymerization of pyrrole.

3.2. ATR-FTIR of nanofibers

In order to confirm the presence of PPy sheath, ATR-FTIR measurements were performed on the electrospun PAN/10 wt% $FeCl_3 \cdot 6H_2O$ nanofibers before and after the surface-initiated polymerization, and the results are exhibited in Fig. 4. For comparison, the FTIR spectrum of pure PAN nanofibers is also shown. It is seen that all of the spectra contain three prominent peaks at around 2930, 2245, and 1450 cm^{-1}, which can be assigned to the stretching vibration of the methylene ($-CH_2-$) group, the stretching vibration of nitrile groups ($-CN$), and the bending vibration of methylene ($-CH_2-$) of PAN, respectively [4,10]. In addition, the intensities of these characteristic peaks increase after the surface-initiated polymerization of pyrrole. Before polymerization, there are intermolecular interactions between PAN and Fe^{3+} ions in electrospun PAN/10 wt% $FeCl_3 \cdot 6H_2O$ nanofibers, such as the coordination of Fe^{3+} ions with $-CN$, or the complex formed by Fe^{3+} ions with both DMF and PAN [30–32], which may lead to relatively weak characteristic peaks at around 2930, 2245, and 1450 cm^{-1}, compared with pure PAN. However, after the surface-initiated polymerization, the PPy sheath is formed and significantly amount of Fe^{3+} ions may be reduced. In addition, the PPy phase may also affect or even inhibit the possible interactions between reduced Fe^{3+} ions and PAN cores. As a result, the former interactions between PAN chains and Fe^{3+} ions decrease, and the intensities of the PAN characteristic peaks increase. It should be noted that the similar report about the interactions between metal ions and PAN/PPy chains

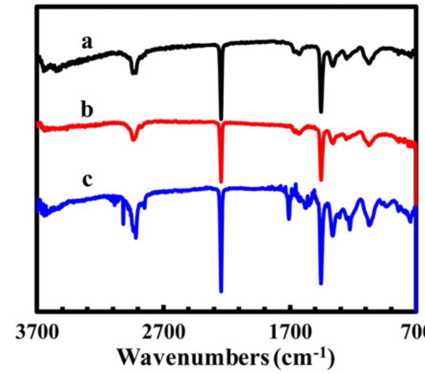

Fig. 4. ATR-FTIR images of (a) pure PAN, (b) electrospun PAN/10 wt% $FeCl_3 \cdot 6H_2O$, and (c) corresponding PAN-PPy core-sheath nanofibers.

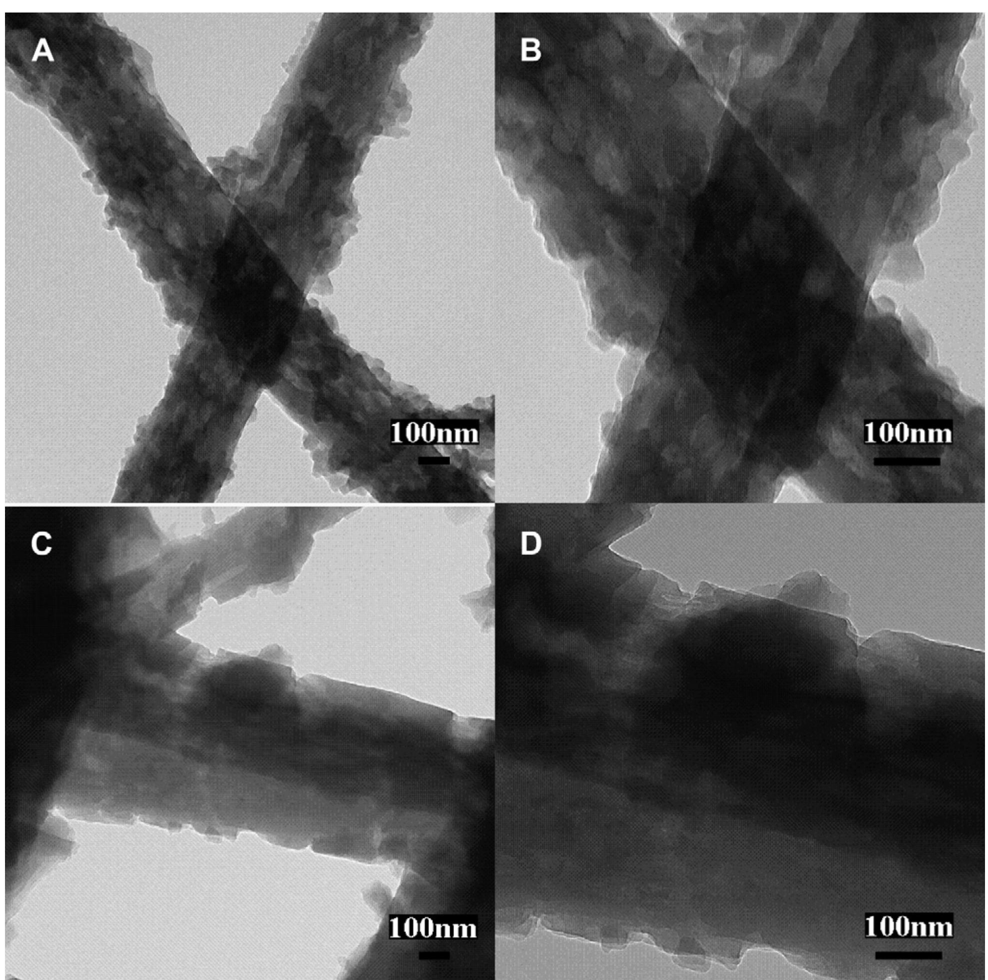

Fig. 3. TEM images of PAN-PPy core-sheath nanofibers made from electrospun PAN/$FeCl_3 \cdot 6H_2O$ with different $FeCl_3 \cdot 6H_2O$ contents: (A, B) 5, (C, D) 10 wt%.

is relatively deficient. Further research along with other characterizations is necessary to identify this issue.

From Fig. 4, it is also seen that after the surface-initiated polymerization, a new peak appears at 1547 cm^{-1}, which may be assigned to the typical PPy ring vibrations. In addition, the peaks at 1178, 1040, and 900 cm^{-1} may correspond to the N–C stretching and the = C–H out-of-plane and in-plane vibrations in PPy, respectively [24,32–35]. The changes in ATR-FTIR spectrum after the surface-initiated polymerization demonstrate that PPy sheath has been formed on the nanofiber surface.

3.3. Thermal analysis of nanofibers

In order to investigate the thermal properties of electrospun pure PAN, PAN/$FeCl_3 \cdot 6H_2O$ nanofibers, and the corresponding PAN-PPy core-sheath nanofibers, DSC and TGA characterizations were performed. Fig. 5 compares DSC thermograms of pure PAN, PAN/10 wt% $FeCl_3 \cdot 6H_2O$, and PAN-PPy core-sheath nanofibers in nitrogen atmosphere. Electrospun pure PAN nanofibers exhibit a relatively large exothermic peak at about 290 °C, which derives from the complex and multiple chemical reactions (*i.e.*, dehydrogenation, instantaneous cyclization, and crosslinking) of PAN during the process of thermal treatment via the free radical mechanism [25,29,30,36,37]. In the presence of Fe^{3+} ions, the exothermic peak shifts to a higher temperature, and the peak also becomes broader compared to that of pure PAN nanofibers. In addition, the peak intensity decreases after the addition of $FeCl_3 \cdot 6H_2O$. The broadening of the exothermic peak in the presence of Fe^{3+} ions suggests that Fe^{3+} ions modify the activity of the free radicals involved in the above-mentioned complex chemical reactions. The decreased peak intensity is due to the interactions between PAN and Fe^{3+} ions (Fig. 4), which inhibit the formation of free radicals on the nitrile groups and subsequent reactions. For PAN-PPy core-sheath nanofibers, the exothermic peak becomes sharper again, and the peak position shifts to a higher temperature of about 320 °C. Similar to the case of PAN/$FeCl_3 \cdot 6H_2O$ nanofibers, the reduced Fe^{3+} ions in PAN-PPy core-sheath nanofibers can also modify and reduce the formation of free radicals involved in the complex chemical reactions. In addition, the coated PPy sheath may also have an inhibit effect on the above-mentioned complex chemical reactions. As a result, the combined contribution of reduced Fe^{3+} ions and PPy sheath retards the formation of free radicals on the nitrile groups of PAN and subsequent re-combinations between the radicals inter- or intra-molecularly, leading to the increase in the exothermic peak temperature for PAN-PPy core-sheath nanofibers [36].

Fig. 6 shows the TGA thermograms of electrospun pure PAN, PAN/10 wt% $FeCl_3 \cdot 6H_2O$, and the corresponding PAN-PPy core-sheath nanofibers under air environment. The TGA thermograms indicate that the thermal stability of PAN/10 wt% $FeCl_3 \cdot 6H_2O$ nanofibers is reduced compared with that of pure PAN nanofibers. For example, the majority of weight loss of pure PAN nanofibers in air occurs in two steps at about 320 and 500 °C, respectively, while PAN/10 wt% $FeCl_3 \cdot 6H_2O$ nanofibers have major weight losses at about 260 and 350 °C, respectively. The reduced stability can be explained by the interactions formed between Fe^{3+} ions and PAN, which accelerate the oxidative stabilization reactions that are known to occur when PAN is thermally treated in an air environment [14,36,38]. In the case of PAN-PPy core-sheath nanofibers, the weight loss temperatures upshift to about 300 and 500 °C, respectively. This may be the result of the combined effects of both PPy and the reduced Fe^{3+} ions. The former is easy to be degraded when thermal treatment in air environment, while the presence of the later can reduce the interactions between Fe^{3+} ions and PAN. These combined effects make the PAN-PPy core-sheath nanofibers decompose at higher temperatures compared with the corresponding PAN/10 wt% $FeCl_3 \cdot 6H_2O$. However, these temperatures are still lower than those of pure PAN.

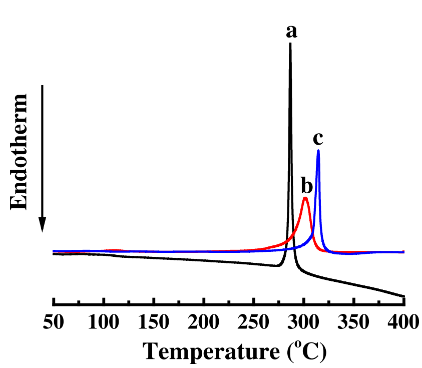

Fig. 5. DSC curves of (a) pure PAN, (b) electrospun PAN/10 wt% $FeCl_3 \cdot 6H_2O$, and (c) corresponding PAN-PPy core-sheath nanofibers.

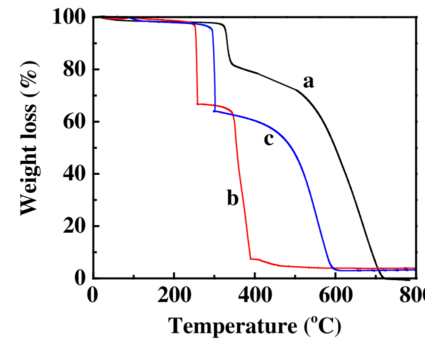

Fig. 6. TGA thermograms of (a) pure PAN, (b) electrospun PAN/10 wt% $FeCl_3 \cdot 6H_2O$, and (c) corresponding PAN-PPy core-sheath nanofibers.

3.4. Surface morphologies of carbonized nanofibers

Fig. 7 shows SEM images of carbon nanofibers obtained by the carbonization of PAN-PPy core-sheath nanofibers. It is seen that these core-sheath nanofiber-driven carbon nanofibers have undulated and wrinkled surface morphology and their diameters are slightly smaller than those of corresponding PAN-PPy core-sheath nanofibers (Fig. 2), which may be due to the liberation of hetero-atoms and the densification of carbon atoms in polymer chains during the thermal treatment [25,29,30,37]. In addition, when PPy/PAN ratio changes in PAN-PPy core-sheath nanofibers, the microstructures of the carbonized nanofibers also change. It should be noticed that PPy is also one important carbon source although it is relatively easy to be degraded when thermally treated in air environment. As a result, these fibers keep their fibrous morphology after the two-step carbonization processes. The prepared CNFs should come from both PPy and PAN components [25]. It is well-known that carbon materials can be used as electrodes in energy storage devices, such as rechargeable lithium-ion batteries and supercapacitors, in which the improvement of the energy density along with other electrochemical performance are strongly dependant on the crystalline phase microstructure and micro-morphology of the carbonaceous material [39]. One-dimensional nanostructured composites have been demonstrated to have suitable structures and functionalities for energy storage [40,41]. We therefore anticipate

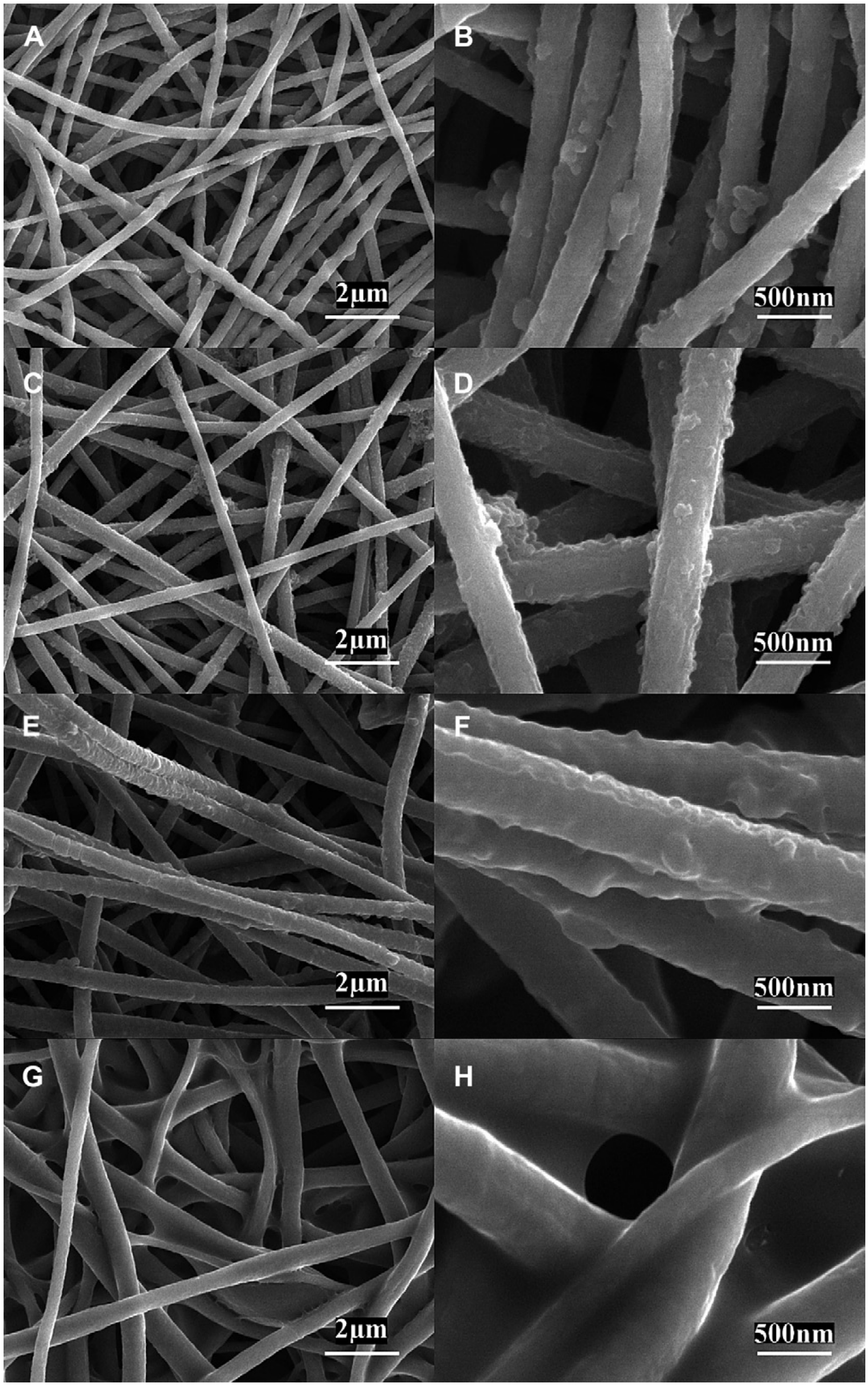

Fig. 7. SEM images of thermally treated PAN/$FeCl_3 \cdot 6H_2O$ composite nanofibers through stabilization and carbonization processes with different $FeCl_3 \cdot 6H_2O$ contents: (A, B) 1, (C, D) 2, (E, F) 5, and (G, H) 10 wt%.

that the special surface morphology and microstructures of the carbon nanofibers derived from PAN-PPy core-sheath nanofiber with different PPy component may have promising electrochemical properties when used as electrodes in energy storage systems.

4. Conclusions

PAN-PPy core-sheath composite nanofibers were prepared by a judicious combination of electrospinning technique and surface-initiated polymerization processes using Fe^{3+} as an oxidant. It was found that with increase in Fe^{3+} content, the PPy sheath structure changes from particle-like, fibrillar, to continuous coating. As-formed core-sheath nanofibers can be thermally treated to prepare carbon nanofibers. Therefore, the combination of electrospinning and surface-initiated polymerization is a feasible approach to prepare conducting core-sheath nanofibers and carbon nanofibers for various applications, including electrodes for energy storage and conversion systems, catalyst supports, sensors, and water purification, etc.

Acknowledgement

This study was supported by the Department of Energy (DE-EE0001177), the U.S. National Science Foundation (No. 0833837), and the ERC Program of the National Science Foundation under Award Number EEC-08212121. The authors would like to thank Mr. Christopher Bonino and Professor Saad A Khan in Chemical and Biomolecular Engineering Department at North Carolina State University for their help in sample characterizations.

References

[1] Ge JJ, Hou HQ, Li Q, Graham MJ, Greiner A, Reneker DH, et al. J Am Chem Soc 2004;126:15754–61.
[2] Hou HQ, Ge JJ, Zeng J, Li Q, Reneker DH, Greiner A, et al. Chem Mater 2005;17:967–73.
[3] Li D, Xia YN. Adv Mater 2004;16:1151–70.
[4] Zhang D, Karki AB, Rutman D, Young DR, Wang A, Cocke D, et al. Polymer 2009;50:4189–98.
[5] Reneker DH, Chun I. Nanotechnology 1996;7:216–23.
[6] Agarwal S, Wendorff JH, Greiner A. Polymer 2008;49:5603–21.
[7] Hong YL, Chen XS, Jing XB, Fan HS, Guo B, Gu ZW, Zhang XD. Adv Mater 2010;22:754–8.
[8] Liu Y, Teng H, Hou HQ, You TY. Biosens Bioelectron 2009;24:3329–34.
[9] Thavasi V, Singh G, Ramakrishna S. Energy Environ Sci 2008;1:205–21.
[10] Ji LW, Medford AJ, Zhang XW. Polymer 2009;50:605–12.
[11] Liu HQ, Reccius CH, Craighead HG. Appl Phys Lett 2005;87:253106.
[12] Formo E, Peng ZM, Lee E, Lu XM, Yang H, Xia YN. J Phys Chem C 2008;112:9970–5.
[13] Huang JS, Hou HQ, You TY. Electrochem Commun 2009;11:1281–4.
[14] Ji LW, Medford AJ, Zhang XW. J Mater Chem 2009;19:5593–601.
[15] Le Viet A, Reddy MV, Jose R, Chowdari BVR, Ramakrishna S. J Phys Chem C Nanomater Interfaces 2010;114:664–71.
[16] Wei M, Lee J, Kang BW, Mead J. Macromol Rapid Commun 2005;26:1127–32.
[17] Wei M, Kang BW, Sung CM, Mead J. Macro Mater Eng 2006;291:1307–14.
[18] Sun ZC, Zussman E, Yarin AL, Wendorff JH, Greiner A. Adv Mater 2003;15:1929–32.
[19] Li D, Xia YN. Nano Lett 2004;4:933–8.
[20] Bognitzki M, Hou HQ, Ishaque M, Frese T, Hellwig M, Schwarte C, et al. Adv Mater 2000;12:637.
[21] Fu GD, Lei JY, Yao C, Li XS, Yao F, Nie SZ, et al. Macromolecules 2008;41:6854–8.
[22] Xu XL, Zhuang XL, Chen XS, Wang XR, Yang LX, Jing XB. Macromol Rapid Commun 2006;27:1637–42.
[23] Dong H, Jones WE. Langmuir 2006;22:11384–7.
[24] Li XF, Hao XF, Yu HB, Na H. Mater Lett 2008;62:1155–8.
[25] Ji LW, Yao YF, Toprakci O, Lin Z, Liang YZ, Shi Q, et al. J Power Sources 2010;195:2050–6.
[26] Xie JW, MacEwan MR, Willerth SM, Li XR, Moran DW, Sakiyama-Elbert SE, Xia YN. Adv Func Mater 2009;19:2312–8.
[27] Chen R, Zhao SZ, Han GY, Dong JH. Mater Lett 2008;62:4031–4.
[28] Laforgue A, Robitaille L. Chem Mater 2010;22:2474–80.
[29] Ji LW, Zhang XW. Nanotechnology 2009;20:155705.
[30] Ji LW, Medford AJ, Zhang XW. J Polym Sci B Polym Phys 2009;47:493–503.
[31] Dong YC, Han ZB, Liu CY, Zhang BH. In: International Conference on Energy Environment Technology (iceet); 2009, vol. 3. p. 218–221.
[32] Sharma R, Lamba S, Annapoorni S. J Phys D Appl Phys 2005;38:3354–9.
[33] Chen W, Li XW, Xue G, Wang ZQ, Zou WQ. Appl Surf Sci 2003;218:215–21.
[34] Nicho ME, Hu H. Sol Energy Mater Sol Cells 2000;63:423–35.
[35] Zhong WB, Liu SM, Chen XH, Wang YX, Yang WT. Macromolecules 2006;39:3224–30.
[36] Kim J, Kim YC, Ahn W, Kim CY. Polym Eng Sci 1993;33:1452–7.
[37] Kim C, Jeong YI, Ngoc BTN, Yang KS, Kojima M, Kim YA, et al. Small 2007;3:91–5.
[38] Dalton S, Heatley F, Budd PM. Polymer 1999;40:5531–43.
[39] Zhou HS, Zhu SM, Hibino M, Honma I, Ichihara M. Adv Mater 2003;15:2107–11.
[40] Zhang Y, Suenaga K, Colliex C, Iijima S. Science 1998;281:973–5.
[41] Schoen DT, Meister S, Peng HL, Chan C, Yang Y, Cui YJ. Mater Chem 2009;19:5879–90.